Impact of relative humidity on a nanostructured filter cake – Experimental and modelling approaches

Q. Ribeyre, A. Charvet, C. Vallières, Dominique Thomas

Impact of Relative Humidity on a Nanostructured Filter Cake - Experimental and Modelling Approaches.

Q. Ribeyre, A. Charvet, C. Vallières, D. Thomas

Laboratoire Réactions et Génie des Procédés, Université de Lorraine, CNRS, UMR 7274, Nancy, F-54000, France

ABSTRACT

In this paper, three different non-hygroscopic nanostructured powders were dispersed in dry air and filtered to create a nanostructured deposit. The relative humidity was then gradually increased from 0 to 85% and the thickness of the deposit continuously measured using a laser trigonometry device. Experimental results showed that for each sample, the pressure drop of the deposit increases when the relative humidity increases, while the bed thickness decreases.

The modelling of the pressure drop upon increasing humidity was conducted using two pressure drop models available in the literature and specifically developed for nanostructured deposits. The variations in porosity and in cake thickness were included in the pressure drop models. This was achieved using a semi-predictive model of adsorption-condensation on nanoparticle beds developed to calculate the water mass sorbed by a powder. The modified models represent the experimental results with a maximum deviation of 10%.

HIGHLIGHTS

► Pressure drop and thickness variations of a humid nanostructured deposit are presented.

► An equation allowing porosity determination for a humid nanostructured deposit is proposed.

► The porosity equation was implemented in two pressure drop models.

► A good match between modelled and experimental results was found.

KEYWORDS

Pressure drop; Porosity, Water sorption isotherm, Non-hygroscopic particles; Multilayer adsorption; Capillary Condensation; Nanoparticles.

NOMENCLATURE

Latin letters

a_0	Water activity	(-)
Cu	Cunningham coefficient	(m)
c_G	GAB energy constant	(-)
d_{pp}	Primary particles diameter	(m)
d_{vg}	Mean geometric volume equivalent diameter	(m)
Fc	Correction factor used in Thomas's model	(-)
H	Deposit thickness	(m)
H_0	Initial deposit thickness	(m)
h	Meniscus demi-width	(m)
k	GAB constant	(-)
m_{bed}	Mass of the dry bed of nanoparticles	(kg)
P	Pressure	(Pa)
r	Meniscus demi-length	(m)
T	Temperature	(K)
t	Thickness of multi-molecular layer	(m)
U_0	Gas velocity	($m\ s^{-1}$)
$V_{particles}$	Total volume of the particles	(m^3)
V_{total}	Total volume of the bed	(m^3)
V_{void}	Total volume of void inside porous medium	(m^3)
V_{water}	Total volume of water sorbed	(m^3)
$v(a_0)$	water mass per sorbent mass	($kg\ kg^{-1}$)
v_{mG}	Quantity of water needed to cover the solid surface with a monomolecular layer	($kg\ kg^{-1}$)
Z	Coordination number	(-)

Greek letters

ΔH	Cake thickness variation	(m)
ΔL	Laser spot variation	(m)
ΔP	Pressure drop	(Pa)
ε	Deposit porosity	(-)
$\vartheta(\varepsilon)$	Void function	(-)
γ	Angle between laser and surface	(°)
μ	Gas viscosity	(Pa s)
Ω	Gas cross-section	(m²)
ρ_l	Liquid density	(kg m^{-3})
ρ_s	Particle density	(kg m^{-3})
σ_g	Geometric standard deviation	(-)
τ	Porous medium tortuosity	(-)

Indices

$_0$	Related to the initial cake parameters	

1. Introduction

In recent years, nanomaterials have known a strong interest all around the world. This development led to an exposure of a growing part of the population to ultrafine particles. For this reason, in recent decades air quality has emerged as a major public environmental and health issue. Despite numerous scientific publications concerning biological and physico-chemical properties of ultrafine particles, we are confronted with a lack of data about potentially induced toxicological risks (Roco et al. 2010). Thus, in most cases, to protect workers and the environment, institutions use Personal Protective Equipment (PPE) and High Efficiency Particulate Air Filters (HEPA) located in the general ventilation circuits. Nevertheless, almost all the available data corresponds to modes with ambient air (ambient temperature and humidity). However, some postulated accident scenarios lead to a high moisture environment (Mocho and Ouf 2011). The interaction of water vapour with particles may significantly affect the performance of such a filtration system. Indeed, if the pressure drop of the filter increase with humidity, it will lead to a reduction of its mechanical resistance and can eventually cause the rupture of the containment. Yet despite these extreme conditions, the HEPA filters used in industrial facilities must maintain their protective role.

Some laboratory measurements have shown that the evolution of the filter pressure drop during loading is strongly impacted by the presence of moisture. The influence of moisture on the pressure drop of a filter during the build-up of the cake is mainly governed by the hygroscopic properties of the aerosol. For a non-hygroscopic aerosol, or a hygroscopic aerosol below its deliquescent point, Gupta et al. (1993) observed a linear increase of the filter pressure drop with collected mass per unit area for micron-sized aluminium oxide (1.19 µm mass median diameter) and for a submicron hygroscopic aerosol of sodium chloride (0.5 µm mass median diameter). The same observations were reported by Miguel (2003) for large-diameter polyester fibre filters loaded with non-hygroscopic (Al_2O_3) or hygroscopic aerosols (NaCl) below their deliquescent point. The results indicated that for the same mass of deposited particles, the filter pressure drop is less important when the humidity increases. For a hygroscopic aerosol at a relative humidity above its deliquescent point, the pressure drop of the filter increases exponentially after a certain mass of droplets has been collected (corresponding to the transition from solid to liquid) (Gupta et al. 1993; Joubert et al. 2010). The same trends were observed by Novick (1992) for micron-sized

sodium chloride and by Vendel and Letourneau (1994) for a metal fibre filter clogged with sodium chloride and caesium hydroxide aerosols.

However, few studies exist in the literature considering the moisture influence on the pressure drop of a deposit built under dry air. In the case of hygroscopic aerosols, most results are related to micron and submicron-sized aerosols. Joubert et al. (2011) studied flat filters loaded with submicron NaCl particles (0.41 µm equivalent volume median diameter) at 0% RH and crossed by humid air below the deliquescent point. When high humidity (RH = 75%) passed through the cake, the authors denoted a decrease in the cake pressure drop, followed by stabilization. Furthermore, Montgomery *et al.* (2015) observed the same trends, but with a depth-loaded filter, a nanostructured NaCl aerosol (approximately 100 nm) and a humidity range between 0 and 60%. For a non-hygroscopic aerosol, Ricketts (1991) and Schröter and Poon (2012) loaded flat filters with a micron-sized atmospheric aerosol (particle size between 100 and 300 nm) and highlighted an increase in the pressure drop after several hours of exposure to a high relative humidity (RH = 90%). Finally, in case of submicron particles, Montgomery *et al.* (2015) investigated the influence of relative humidity (between 0 and 60%) on the pressure drop of flat air filters depth-loaded with Al_2O_3 particles (approximately 400 nm). After loading at a specified humidity, they exposed the filters to clean air. No change in the pressure drop were seen with relative humidity changes, even when the relative humidity of the clean air for exposure was higher than that during loading for filter media. Experiments were also conducted with mixtures of hygroscopic (NaCl – 100 nm number median diameter) and non-hygroscopic (Al_2O_3 – 400 nm number median diameter) particles to simulate real air systems (atmospheric aerosols). The changes in filter performance characteristics were higher for an aerosol mainly composed of hygroscopic particles than for one that was mainly a non-hygroscopic aerosol. In other words, the change in the pressure drop was lowest for 100% Al_2O_3 particles. The impact of exposure to humidity was a function of filter media and dust loading level, as well as exposure to relative humidity. The authors postulated that particles captured within the filter media while loading at low humidity underwent growth in particle size when exposed to higher humidity. This increase in particle size could impose stress on the structure, resulting in physical restructuring of the particles in the fibers.

Though the studies detailed above have indicated trends in terms of pressure drop for hygroscopic and non-hygroscopic particles, no definite conclusions could be drawn about the effects of relative humidity

on the pressure drop of the deposit. Furthermore, the humidity effects are bound to depend on the aerosol material's properties, such as hygroscopicity, and particle size of the aerosol. Thus, the interactions between water vapour and particles composing the cake should be responsible for these variations. However, it is not entirely clear how these phenomena impact the cake pressure drop. Moreover, the studies described above principally concern the submicron or micron-sized aerosols, and almost no information is available in the literature regarding nanostructured particles.

For these reasons, the first objective of this study was to determine the effects of humidity on the pressure drop of a nanostructured deposit formed under dry air by non-hygroscopic particles. The second objective aimed to provide explanations of the observed trends. Hence, part of the study was devoted to the investigation of the thickness and mass variation of the bed under humid conditions. Then, the cake porosity was evaluated using thickness variations and an Adsorption-Condensation Model (ACM) developed in a previous study (Ribeyre et al. 2014). Finally, a pressure drop model that took into account the cake porosity and cake thickness under humidity was proposed and compared to experimental data.

2. Experimental description

2. 1. Sample characterization

Three kinds of non-hygroscopic agglomerates, consisting of nearly spherical nanoparticles were used I this study:

- Zinc-aluminium (from metallisation fumes) generated by an electric arc gun.
- Amorphous carbon (named Xe2 PRINTEX) provided by Orion Engineering Carbons, Frankfurt, Deutschland.
- Aerosil 200 (fumed silica), provided by Evonik Industries, Essen, Deutschland.

The particle size analysis of the tested powders were determined using a 120 kV Zeiss®, EM 910 model transmission electron microscope (TEM). Densities were measured by a helium pycnometer (Micromeritics®, AccuPyc 1330 model), and compositions were given by the supplier:

	Particle diameters		Density ρ_s (kg m^{-3})	Composition (%)
	Number mean diameter (nm)	Standard deviation		
Zinc-Aluminium	21	5	5720	85 % zinc 15 % aluminium
Xe2 PRINTEX	71	18	2350	97.6 % carbon 0.81 % oxygen
Aerosil 200	19	4	2580	> 99.8 % SiO_2

Table 1. Sample characterizations.

To understand the cake behaviour under humidity, the water mass sorbed by each sample is an undeniable asset. A Setaram microbalance and a Wetsys_ generator were used to determine the powders' sorption isotherms. The experimental protocol described in Ribeyre et al. (2014) was used to obtain the water mass sorbed by these samples. Fig. 1 presents the experimental and modelled mass of water sorbed by mass of dry sample versus the water activity:

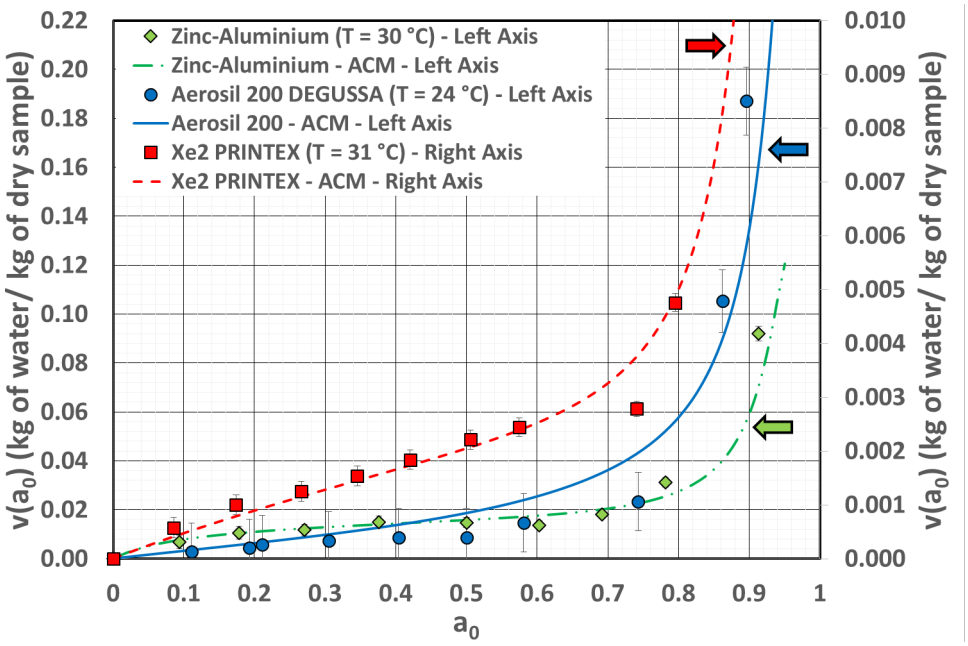

Figure 1. Zinc-Aluminium, Aerosil 200 and Xe2 PRINTEX water sorption isotherms (Ribeyre et al. 2014).

These type II isotherms are obtained with non-porous sorbents or macro-porous materials, where the adsorbed layer gradually increases. Aerosil 200 has the strongest affinity for water, followed by Zinc-Aluminium and Xe2 PRINTEX. Beyond a water activity of 0.7, each sample shows a rapid increase of the sorbed amount. Proving that, capillary condensation was the dominant phenomenon rather than multilayer adsorption (Ribeyre et al. 2014).

The water sorption model is based on the theory of multi-molecular adsorption (Timmermann 2003) combined with the capillary condensation phenomenon (Kelvin's law). The condensation part takes into account the formation of an adsorbed layer (of thickness denoted t) at the surface of each particle (Ribeyre et al. 2014). In this model, the particles are assumed to be spherical, non-porous and in contact with each other (no distance between particles). Moreover, the surface of the liquid in contact with the air is taken to be planar (*i.e.* the meniscus between this surface and the spheres is neglected).

Therefore, the final equation of the Adsorption-Condensation model (AC Model) is as follows:

$$v(a_0) = \frac{v_{mG}\, c_G\, a_0\, k}{(1 - k\, a_0)(1 + (c_G - 1)k\, a_0)} + Z\, \frac{\rho_l}{\rho_s}\left[3\left(\frac{h - t}{d_{pp}}\right)^2\left(1 - \frac{4\,(h - t)}{3\, d_{pp}}\right)\right] \qquad (1)$$

With this equation, it is possible to represent the experimental isotherm over the whole range of water activity. The porosity, density and diameter of the primary particles composing the bed are needed to estimate $v(a_0)$. It is worth noting that v_{mG}, c_G and k were determined by graphical fitting (following IUPAC recommendations); the coordination number (Z) and the thickness of the multi-molecular layer (t) were determined by calculation (Ribeyre et al. 2014). The coordination number (Z) is determined by an empirical correlation as a function of cake porosity and can vary by a factor of two in the several expressions found in the literature. In this paper, the used empirical correlation is the Meissner at al. (1964) one giving a mean value of Z.

The fitted parameters are given in Table 2 for the three samples:

Sample	v_{mG} (kg of water/kg of dry sample)	c_G	K
Zinc-Aluminium	1.05×10^{-2}	60.36	0.675
Xe2 PRINTEX	2.01×10^{-3}	8.78	0.500
Aerosil 200	5.21×10^{-3}	12.97	0.611

Table 2. AC Model Parameters for the samples (Ribeyre et al. 2014).

2. 2. Materials & Methods

To record pressure drop variations of a nanostructured deposit under various moisture levels, an experimental set-up was developed. This is divided into three parts (Figure 2):

- An aerosol production zone, which allows the generation of particles.
- A humidification zone, which creates a humidity controlled environment.

- A measurement zone consisting of a series of various sensors that record simultaneously: the moisture content of the exhaust gas, the cake thickness and the pressure drop.

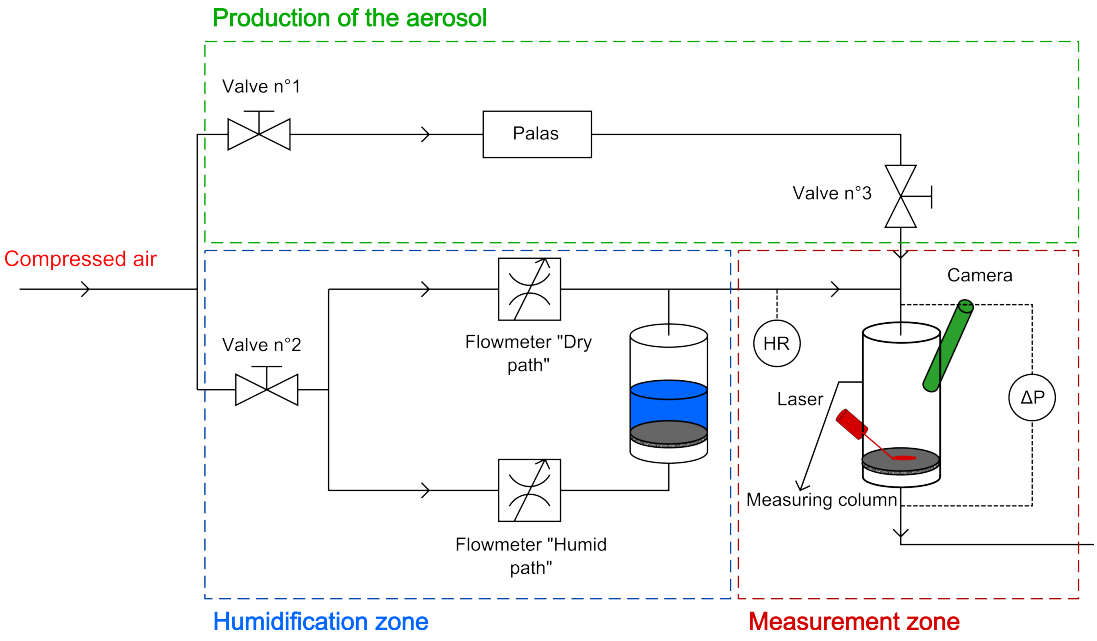

Figure 2. Schematic diagram of the experimental set-up.

An aerosol generator (Palas RBG 1000) was used to produce the nanostructured particles that were collected on a sintered plate. The pressure drop of this support was recorded at a water activity of 0.85 for 70 hours in order to control the humidity effect. No pressure drop variation was observed.

By using two mass flowmeters (Brooks® SLA 5850 S) and a bubbler, the humidity can be controlled from 0 to 85 % at a total flow rate of 2.6 L min^{-1}.

A capacitive relative humidity sensor with an accuracy of ±2% was placed at the inlet of the measurement column and a differential pressure transmitter (Keller PD 33 X with an accuracy of ±15 Pa of the reading over the entire range) was used for the determination of the cake pressure drop.

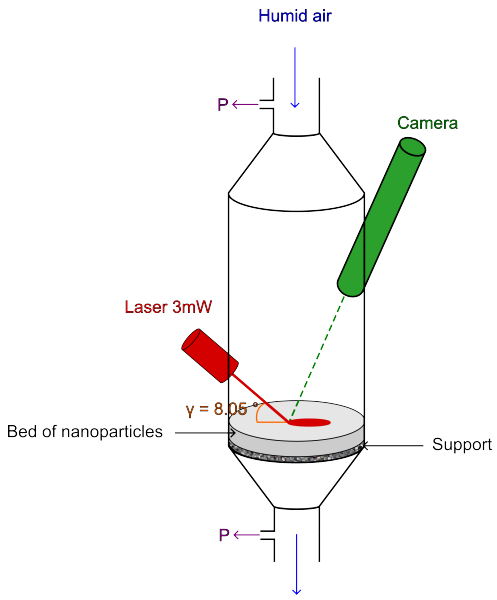

Figure 3. Schematic picture of the measurement column.

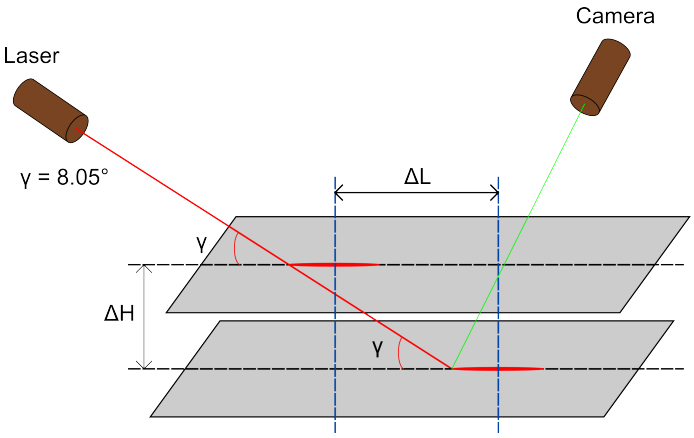

Figure 4. Principle of the laser thickness measurement

An experimental setup inspired by the study of Altmann and Ripperger (1997) was developed to determine the cake thickness. This device is composed of a 10 cm high column containing a metallic sintered support, with a 47 mm inner diameter, to carry the nanostructured deposit (Fig. 3).

A laser (power of 3mW and wavelength 635nm) impacted the surface of particle cake with an angle γ of 8.05° and a microscopic camera (SuperEyes®) recorded laser displacements. A cake thickness modification ΔH (Figure 4) can be obtained by a simple trigonometric formula from the measurement of the laser spot displacement ΔL:

$$\Delta H = \Delta L \tan \gamma \qquad (2)$$

The laser displacement is obtained from pictures recorded by the camera and processed using the Matlab software ®. Pixels with maximum intensity are selected using a binary procedure. This technique allows an intensity of 1 to be attributed to the laser spot, while the background intensity is set to 0. Then, the barycentre coordinates of the laser spot are calculated. Knowing its position between two pictures, it is possible to determine ΔH, the bed thickness variation (using equation 2). The measurement error depends on the camera resolution and on pixel size, equal to 11.7µm in this study. Thus, in these conditions, the minimal cake thickness variation is 11.7µm.

The laser trigonometry method is a local analysis technique. In this study, we assume that the local measured thickness is equal to the deposit thickness (in other words we assume a flat filter cake). However, this technique may be slightly affected by the particle composition. The black colour of the

aerosol (like Xe2 PRINTEX) can be a problem for the laser trigonometry method. Indeed, during generation, this powder tends to mask the laser spot and reduce the intensity measured by the camera. To improve the measurement, the pictures are treated using seven different binarization conditions. The cake thickness is calculated with the method described above for every binarization condition and the average thickness is reported.

Concerning experimental procedures, nanoparticle cakes are created by filtration at 15 L min^{-1} (14.4 cm s^{-1}) until their thicknesses reach about 1 to 3 mm. When the aerosol generation is stopped, a flow of dry air of 2.6 L min^{-1} (2.55 cm s^{-1}) is sent through the nanostructured deposit. A lower permeation flow is used to avoid potential bed compression issues. When the pressure drop remains stable, this value and the cake thickness are recorded. The air humidity is then increased until a new equilibrium is reached and previous steps are repeated for the whole range of humidity. At the end of the experiment, the cake is weighed and dried in a heat chamber to calculate the final porosity.

3. Modelling

The main objective of this study was to predict the evolution of the pressure drop across a filter cake, as a function of the air moisture content. Two versions of a developed model are presented, each deriving from a pressure drop model available in the literature (Endo et al., 2002 and Thomas et al., 2014). The influence of moisture content will be taken into account using the AC model described in a previous study (Ribeyre et al. 2014). Using this model it is possible to estimate the cake porosity under moisture conditions, and finally to insert these data into the pressure drop models.

3. 1. Pressure drop models

Several studies of the permeability of particle packed beds are reported in the literature, but few of them concern nanostructured deposits. Only two models validated with nanostructured deposits can be listed: the Endo and Thomas models.

3. 2. 1. Endo et al.'s model

Endo's particulate model was developed for laminar flows (Endo et al. 2002). A study has been carried out by the authors to highlight the application limit of the Kozeny-Carman equation in the case of beds

having a wide particle size distribution and/or non-spherical particle shape. With the assumption of log normal particle size distribution, and using the so-called channel and drag theory, the authors showed that the pressure drop of the porous medium can be expressed as follows:

$$\Delta P = 18\,\mu\,U_0\,H\,\frac{(1-\varepsilon)\,\vartheta(\varepsilon)}{Cu\,\varepsilon^2}\,\frac{k}{d_{vg}^2\,\exp(4\,\ln^2\sigma_g)} \quad (3)$$

In a dimensionless form:

$$\frac{\Delta P}{\Delta P_0} = \frac{H}{H_0}\,\frac{(1-\varepsilon)\,\varepsilon_o^2\,\vartheta(\varepsilon)}{(1-\varepsilon_0)\,\varepsilon^2\,\vartheta(\varepsilon_o)} \quad (4)$$

Where the 0 index is related to the initial cake (that formed at relative humidity close to 0%). k, the dynamic shape factor is set to 1 since the primary particles are nearly spherical. d_{vg}, is the mean geometric volume equivalent diameter. σ_g, the geometric standard deviation. Cu, the Cunningham coefficient (Kim et al. 2005). The void function, $\vartheta(\varepsilon)$, indicates the effects of neighbouring particles and takes into account the change in fluid apparent viscosity depending on the porosity or particle concentration (Kim et al. 2009). In this paper, the following void function is used:

$$\vartheta(\varepsilon) = \frac{10\,(1-\varepsilon)}{\varepsilon} \quad (5)$$

It is important to note that in the case of monodisperse and spherical particles, the combination of equations 3 and 5 represents the Kozeny-Carman equation.

3. 2. 2. Thomas et al.'s model

Thomas' model calculates the pressure drop of a nanostructured deposit in the case of laminar flow (Thomas et al. 2014). Since the structure of nanoparticle deposits can be assimilated as dendritic forms and since such cakes present very high porosity, the authors have postulated that it is more appropriate to use drag force acting on the "particle chains". Thus, the nanostructured deposit can be assimilated as a tangle of chains composed of juxtaposed particles or partially overlapping ones. The model equation is as follows:

$$\Delta P = \frac{64\,(1-\varepsilon)^{3/2}\,(1+56\,(1-\varepsilon)^3)\,\mu\,U_0\,H\,F_C}{Cu\,d_{pp}^2} \quad (6)$$

This model takes into account the total length of the particles chains (calculated from the cake packing density, the primary particle diameter and the partial overlap between particles) and the drag force per unit length of fiber (estimated from the Davis equation). To express the importance of particle overlap,

the authors propose to introduce a correction factor F_C, equal to 3/2 for juxtaposed particles with no overlap. Finally we can express the equation above in a dimensionless form:

$$\frac{\Delta P}{\Delta P_0} = \frac{(1-\varepsilon)^{3/2}\,[1+56\,(1-\varepsilon)^3]H}{(1-\varepsilon_0)^{3/2}\,[1+56\,(1-\varepsilon_0)^3]\,H_0} \tag{7}$$

3. 2. Modelling approach

To represent the experimental data of the pressure drop changes under the influence of humidity it was assumed that the water sorbed in the porous medium is the main phenomenon responsible for variations in pressure drops. Indeed, when a large amount of water is sorbed by the particles, it will form an adsorbed layer and capillary bridges between particles. This will lead to a reduction of the cross-section of the gas. Thus, to introduce these changes in the pressure drop models described above, a new bed porosity must be calculated (Fig. 5).

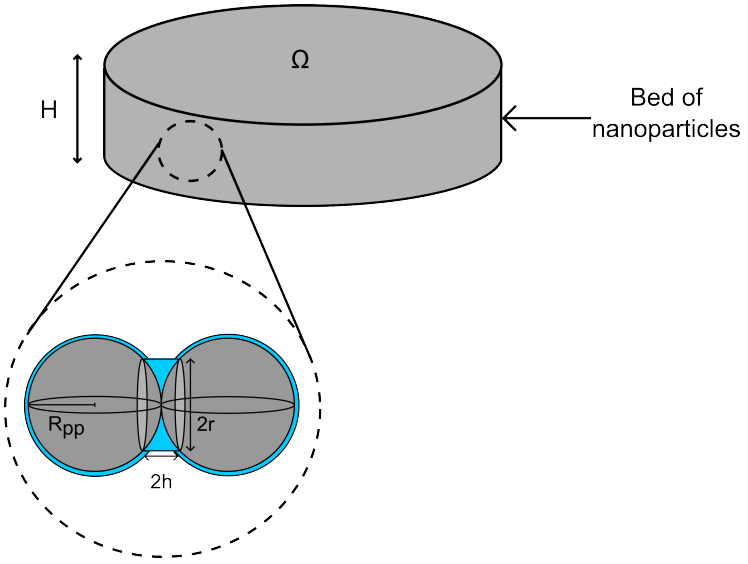

Fig 5. Wet bed of nanoparticles.

The porosity is the ratio between the volume of the pores and the total volume of the bed.

$$V_{total} = V_{void} + V_{particles} + V_{water} \tag{8}$$

Where $V_{particles}$ and V_{water} are respectively the total volume of the particles and the volume of water sorbed by the sample (m^3), which can be calculated as follows:

$$V_{water} = \frac{v(a_0)\,m_{bed}}{\rho_l} \tag{9}$$

Where m_{bed} is the mass of the dry bed of nanoparticles (kg). As we can see from equation 9, the water volume is indeed proportional to $v(a_0)$, which is given by equation 2. The final equation of the cake porosity is given by equation 10:

$$\varepsilon(a_0) = 1 - \frac{H_0}{H}(1 - \varepsilon_0)\left(1 + \frac{\rho_S}{\rho_L} v(a_0)\right) \quad (10)$$

It is worth noting that this equation requires the determination of the thickness of the porous medium (denoted H) which is dependent on water activity and knowing the mass of sorbed water by a given mass of dry sample.

4. Results and Discussion

4. 1. Experimental results

For comparison purposes, the relative pressure drop ($\Delta P/\Delta P_0$) at equilibrium versus water activity are represented in Figure 6 for Zn-Al, Aerosil 200 and Xe2 PRINTEX. The pressure drop of the sintered support is subtracted from the total pressure drop so that ΔP and ΔP_0 reflect only the particle deposit.

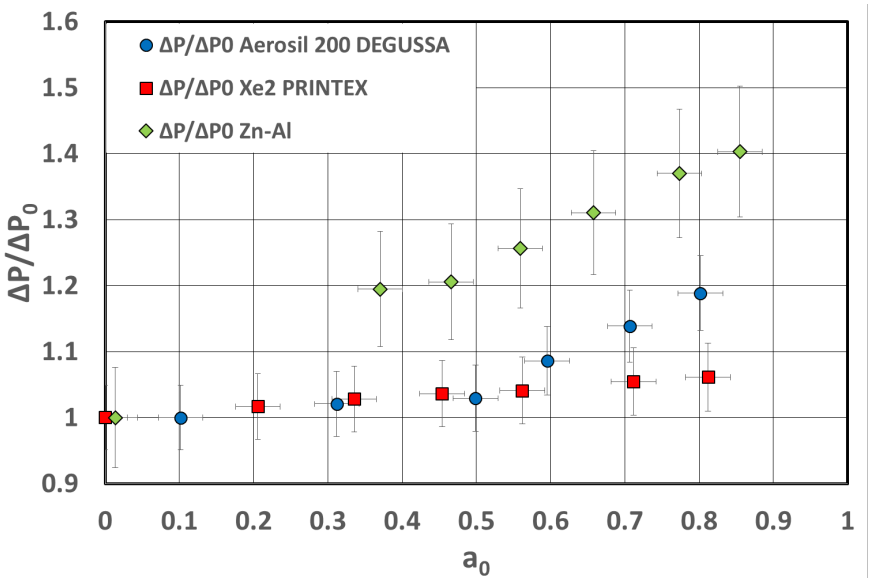

Fig 6. Relative pressure drop versus water activity for each sample.

Figure 6 shows that the zinc-aluminium cake presents the highest increase in pressure drop (40% for a_0 = 0.85). However, for the same moisture content, Aerosil 200 shows a relative pressure drop increase of 20%. Finally, Xe2 PRINTEX is less impacted by high water activity (with less than 5% increase for RH = 80%).

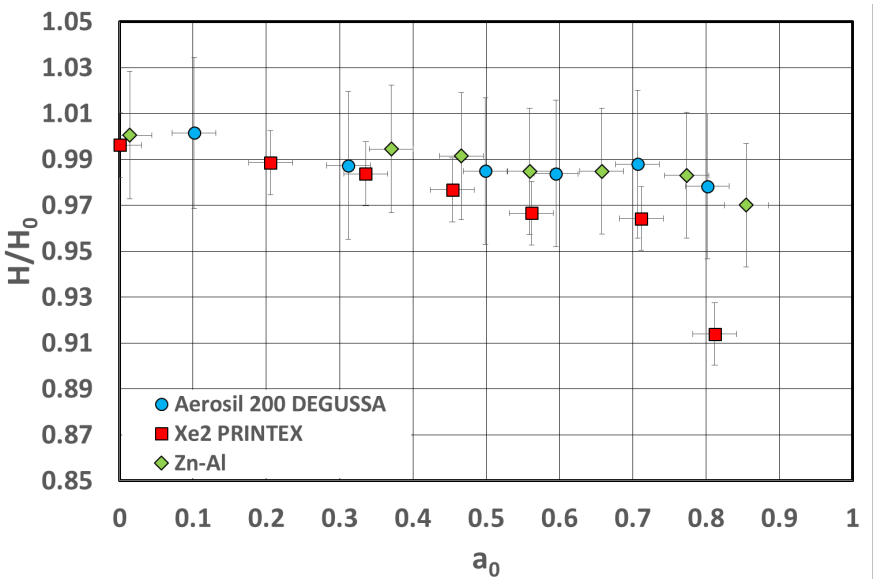

Fig 7. Relative thickness versus water activity for each sample.

Figure 7 represents the relative thickness versus water activity for each sample, and indicates that an increase in the moisture content leads to a slight decrease of the thickness for each sample (approximately 3% for a_0 = 0.7). However, for Zn-Al and Aerosil 200 samples, regarding error bars, each sample has similar thickness variations. In the tested water activity range, the highest cake height reduction is obtained for Xe2 PRINTEX sample (nearly 10% at a_0 = 0.82). This evolution cannot be attributed to cake compression, because the final pressure drop (at RH = 80% at a total flow rate of 2.6 L min^{-1}) is lower than the pressure drop denoted at the end of clogging (at a total flow rate of 15 L min^{-1}). The slope is higher above 70% RH, corresponding to the beginning of the capillary condensation phenomenon (Ribeyre et al. 2014). These results clearly show that increasing moisture modifies the deposit structure. To explain this, we assume that the water adsorption on the particle surface (at low RH values) and the liquid bridges between particles formed by condensation (for RH > 70%) modify internal forces of the nanostructured deposit.

Figure 8 shows the deposit porosity (calculated using equation 10) versus water activity for every sample. The crosses indicate the porosity determined at the end of the experiment by comparison of the wet and dry masses of samples.

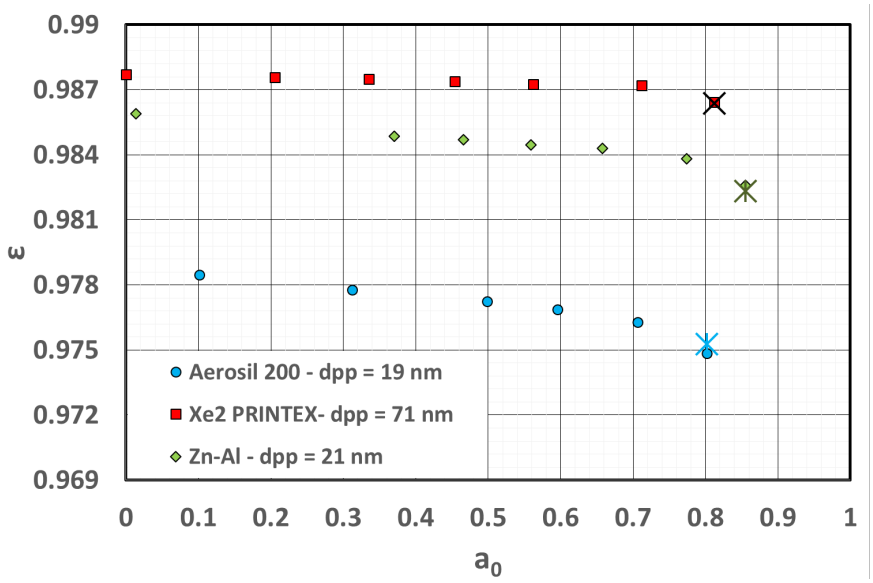

Fig 8. Calculated porosity (equation 10) versus water activity for the three samples and for the median particle diameters.

The deposit porosity decreases while water activity increases. Zn-Al and Aerosil 200 samples show the highest variation (a decrease of 0.3 and 0.4% of the initial value, respectively). Xe2 PRINTEX porosity is less affected by the moisture content, with a maximum diminution of 0.1%. For all samples, the highest porosity variation appears above 70% RH, corresponding to the beginning of capillary condensation. For each sample, the calculated porosity at the end of the experiment is in agreement with that obtained from gravimetric measurements.

The experimental results presented here allow expanding the understanding of pressure drop variations under moist conditions. In the surface loading case, the pressure drop increases when the filter cake becomes denser, as observed in this study. This fact may be explained by the growth of the interparticle forces under humidity (Butt and Kappl 2009) which decrease the total volume of the cake and consequently the porosity. More precisely, for the whole humidity range, the adsorption phenomenon reshapes the deposit resulting in a porosity diminution. For high humidity (> 70%) the capillary condensation phenomenon becomes predominant, thus water fills the pores between particles. The combination of these two effects (condensation and deposit collapse) increase the porosity reduction phenomenon.

However, in the depth-loading case, Montgomery et al. (2015) observed no pressure drop variation after exposure to humidity if the filter is clogged by a non-hygroscopic aerosol. As, the authors only studied

the influence of humidity, between 0 and 60%, they probably cannot observe the influence of the capillary condensation.

4. 2. Models

The experimental pressure drops were compared with those calculated by the two pressure drop equations 4 and 7. To model the pressure drop changes under the influence of moisture, we took into account in these equations the experimental thickness values obtained by laser trigonometry and the cake porosity (equation 10). The two models were considered for three values of particle diameter d_{pp} (the number mean diameter ± standard deviation). The primary particle diameter is one of the most important parameters in the Adsorption-Condensation model. Indeed, when the particle size decreases, a higher number of particles form the same mass of particle bed. This increase in the number of particles significantly increases the total number of contact points and leads to a greater volume of condensed water between the particles which constitute the sample. Therefore, the cross-section of the fluid will be reduced and according to equation 10, the porosity will decrease, resulting in a higher pressure drop.

Figures 9, 10 and 11 compare the experimental and calculated pressure drops obtained respectively with Zn-Al, Xe2 PRINTEX and Aerosil 200 samples. Experimental data are well represented by both models. A rapid increase in the pressure drop can be observed beyond an activity of 0.7-0.8. This may be explained by capillary condensation, which becomes the dominant phenomenon rather than multilayer adsorption, and leads to a major porosity decrease. Whatever the model used, the influence of primary particle diameter is only consistent with a high water activity (*i.e.* when capillary condensation occurs).

Regarding deviation between the models and the experimental data, for Aerosil 200, the models overpredict the experimental data. This is the opposite, for Zn-Al sample. This observation may be explained by the difficulty of modelling water sorption isotherms, especially for high humidity values. Indeed, for high water activities, the modelling is dependent of coordination number (Z) which is determined by an empirical correlation depending on cake porosity. This coordination number can vary by a factor of two in the several expressions found in the literature. In this paper, the Meissner at al. (1964) empirical correlation is used, as it gives a mean value of Z. Nevertheless, using another correlation of the coordination number may involve a slight modification of the $\Delta P/\Delta P_0$ evolution.

Moreover, as the models are global, they do not take into account the local heterogeneities due to local variation of porosity which can explain the differences between experimental and calculated values.

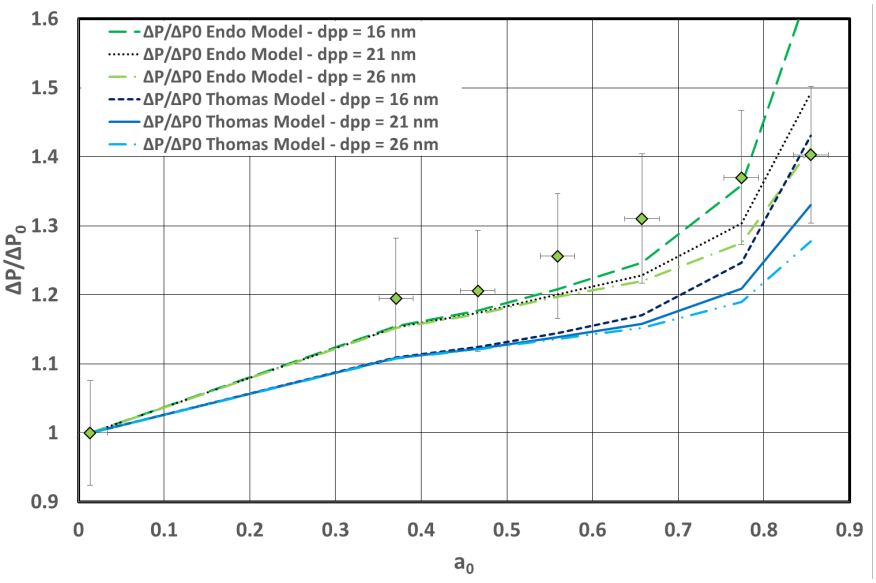

Fig 9. Experimental and calculated pressure drops as function of water activity for the Zn-Al sample.

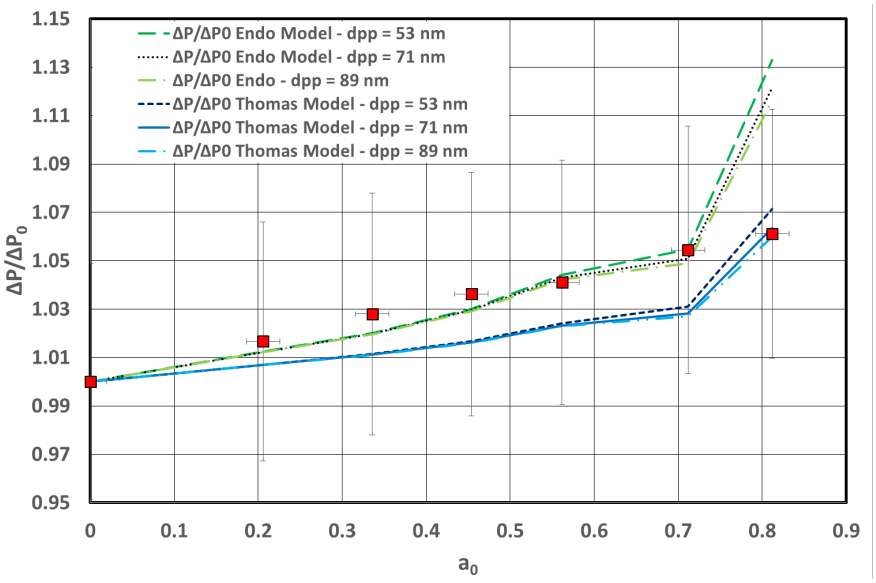

Fig 10. Experimental and calculated pressure drops as function of water activity for the Xe2 PRINTEX sample.

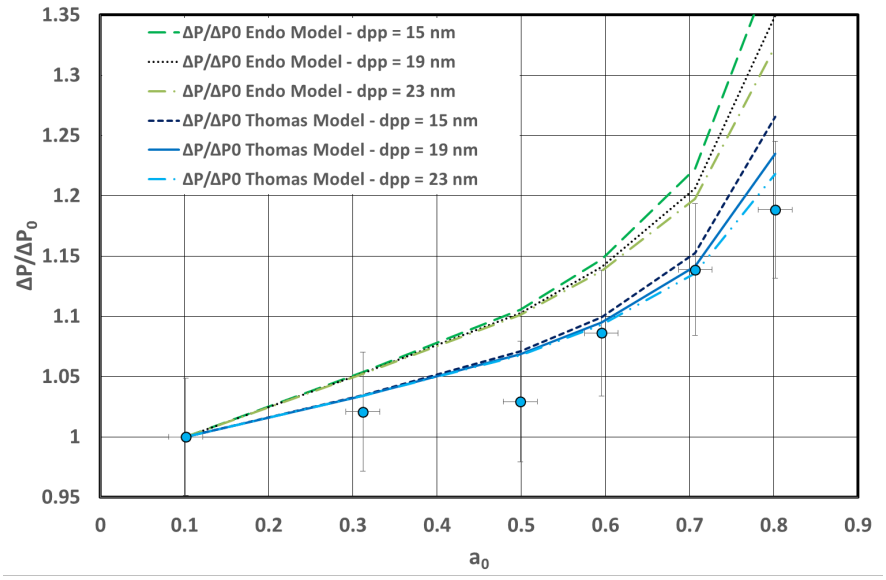

Fig 11. Experimental and calculated pressure drops as function of water activity for the Aerosil 200 DEGUSSA sample.

To quantify the difference between experimental and theoretical data, experimental versus relative theoretical pressure drops were represented for each model. Only median primary particle diameters are taken into account. The parity line and a variance of ± 5 and 10 % from this line were also represented (Figure 12):

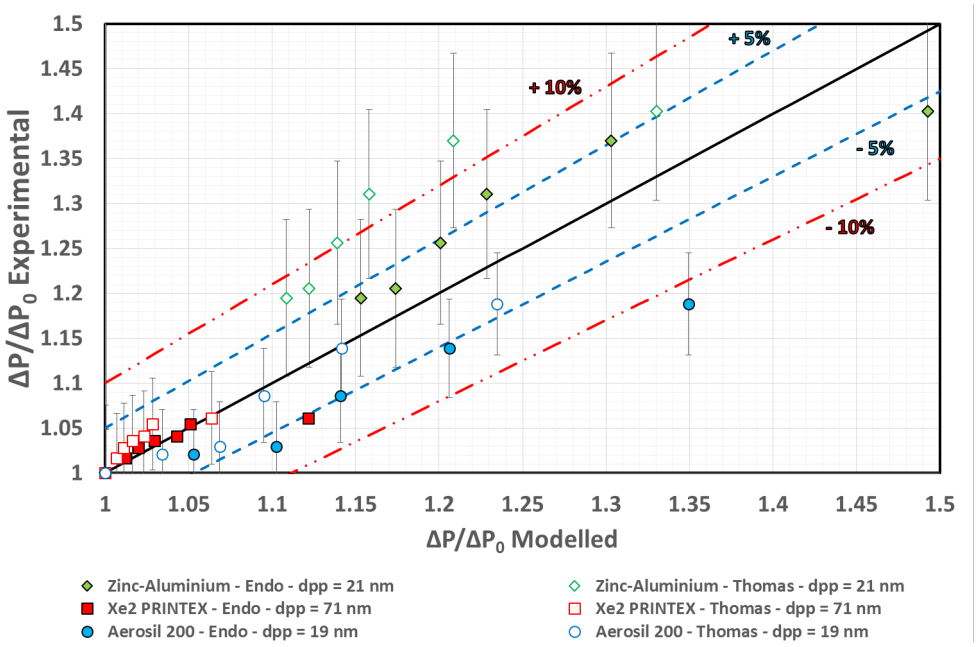

Fig 12. Comparison between experimental and calculated pressure drop values for the three samples.

The models have been tested on a large range of water activity and for various physical powder characteristics (primary particle sizes, cake porosity) and chemical composition (taken into account in the water sorption isotherms). Considering the measurement uncertainties, the agreement between modeled and experimental data seems good (maximum deviation of 10%) whatever these particles types. Only the Endo model for Aerosil 200 and the Thomas model for Zn-Al are located slightly away from the 10% parity line. It is important to note that the large size of error bars prevents objective definition of the most accurate model. Based on these observations, adsorption and condensation (which induce cake porosity and thickness changes) can be considered as the predominant phenomena explaining the pressure drop increase.

5. Conclusions

The purpose of this work was to investigate the impact of relative humidity changes on the pressure drop of a nanostructured deposit. For the three non-hygroscopic samples studied, the pressure drop increases with RH. For high RH (85%), the ratio of ΔP (at considerable RH values) and $\Delta P0$ (at RH = 0%), can reach 1.4. An experimental set-up based on a laser measurement allowed the determination of the deposit thickness at different relative humidities. These results clearly showed a decrease in thickness when humidity is increased, and therefore a deposit structure modification. To explain this phenomenon, we assumed that the water adsorption onto the particle surface (for low RH values) and the liquid bridges between particles formed by condensation (for RH values higher than 70%) modified the internal forces of the nanostructured deposit. Two pressure drop models validated with nanostructured deposits have been tested assuming a deposit of spherical and non-porous particles. The deposit porosity was calculated taking into account changes in the cake thickness and the volume of the adsorbed/condensed water according to the relative humidity value.

A sensitivity analysis of these models has been effected regarding primary particle diameters. It was found that this is an important parameter for models. When the particle size decreases, it will create a higher number of particles for the same mass of particle bed. This increased number of particles will significantly increase the sorbed/condensed water mass and will lead to a higher increase in pressure drop. Whatever the pressure drop model, the agreement between experimental and calculated values is fairly good. The large majority of experimental values are within the range of plus or minus 10% of the theoretical value. Unfortunately, the use of these models requires the knowledge of the water sorption

isotherm to obtain the three GAB constants taking part in the water adsorption-condensation model described in a previous study (Ribeyre et al. 2014) and the deposit thickness variation with RH.

Acknowledgements

This work is a part of the LIMA joint research program between the Institut de Radioprotection et de Sûreté Nucléaire (IRSN) and the Reactions and Chemical Engineering Laboratory (LRGP) of the French National Centre for Scientific Research (CNRS) and the Lorraine University.

References

Altmann J, Ripperger S (1997) Particle deposition and layer formation at the crossflow microfiltration. *J Membr Sci 119–128.*

Butt H-J, Kappl M (2009) Normal capillary forces. Adv Colloid Interface Sci 146:48–60.

Endo Y, Chen D-R, Pui DYH (2002) Theoretical consideration of permeation resistance of fluid through a particle packed layer. *Powder Technol 124:119–126.*

Gupta A, Novick VJ, Biswas P, Monson PR (1993) Effect of Humidity and Particle Hygroscopicity on the Mass Loading Capacity of High Efficiency Particulate Air (HEPA) Filters. *Aerosol Sci Technol 19:94–107.*

Joubert A, Laborde JC, Bouilloux L, Callé-Chazelet S, Thomas D (2010) Influence of Humidity on Clogging of Flat and Pleated HEPA Filters. *Aerosol Sci Technol 44:1065–1076.*

Joubert A, Laborde JC, Bouilloux L, Chazelet S, Thomas D (2011) Modelling the pressure drop across HEPA filters during cake filtration in the presence of humidity. *Chem Eng J 166:616–623.*

Kim JH, Mulholland GW, Kukuck SR, Pui DYH (2005) Slip correction measurements of certified PSL nanoparticles using a nanometer differential mobility analyzer (Nano-DMA) for Knudsen number from 0.5 to 83. *J Res Natl Inst Stand Technol 110:31–54.*

Kim SC, Wang J, Shin WG, Scheckman JH, Puy DYH (2009) Structural Properties and Filter Loading Characteristics of Soot Agglomerates. *Aerosol Sci Technol 43:1033–1041.*

Miguel A. (2003) Effect of air humidity on the evolution of permeability and performance of a fibrous filter during loading with hygroscopic and non-hygroscopic particles. *J Aerosol Sci 34:783–799.*

Mocho VM, Ouf F-X (2011) Clogging of industrial pleated high efficiency particulate air (HEPA) filters in the event of fire. *Nucl Eng Des Vol. 241:p. 1785–1794.*

Montgomery JF, Green SI, Rogak SN (2015) Impact of Relative Humidity on HVAC Filters Loaded with Hygroscopic and Non-Hygroscopic Particles. *Aerosol Sci Technol 49:322–331.*

Novick VJ, Monson PR, Ellison PE (1992) The effect of solid particle mass loading on the pressure drop of HEPA filters. *Journal of Aerosol Science, 23, 6, pp 657-665.*

Ribeyre Q, Grévillot G, Charvet A, Vallières C, Thomas D (2014) Modelling of water adsorption–condensation isotherms on beds of nanoparticles. *Chem Eng Sci 113:1–10.*

Ricketts CI (1991) Mathematical models for changes in HEPA filter pressure drop caused by high air humidity. *21st DOE/NRC Nuclear Air Cleaning Conference. San Diego, California, p. 671–694*

Roco M, Mirkin CA, Hersam MC (2010) WTEC Panel Report on: *Nanotechnology Research Directions for Societal Needs in 2020.*

Schröter M, Poon W (2012) Effects of humidity on the removal efficiencies of submicron particles for clean and real-world loaded air filters. *11th World Filtration Congress, - Session G18 - Filter Media I, Australia.*

Thomas D, Ouf FX, Gensdarmes F, Bourrous S, Bouilloux L (2014) Pressure drop model for nanostructured deposits. *Sep Purif Technol 138:144–152.*

Timmermann E (2003) Multilayer sorption parameters: BET or GAB values? Colloids Surf Physicochem *Eng Asp Vol. 220:p. 235–260.*

Vendel J, Letourneau P (1994) Effect of humidity on the filter pressure drop. *Nuclear Air 23rd DOE/NRC Cleaning and Treatment Conference. pp 187–194.*